Dynamic fracture analysis by explicit solid dynamics and implicit crack propagation

DOI:
10.1016/j.ijsolstr.2017.01.035

Document Version
Submitted manuscript

Dynamic fracture analysis by explicit solid dynamics and implicit crack propagation

Timothy Crump[1], Guilhem Ferté[2], Andrey Jivkov[1], Paul Mummery[1], Van-Xuan Tran[1]

[1] Modelling and Simulation Centre, MACE, University of Manchester, Sackville Street, Manchester, UK

[2] EDF R&D, 7 Boulevard Gaspard Monge, 91 120 PALAISEAU, France

ABSTRACT

Combining time-dependant structural loading with dynamic crack propagation is a problem that has been under consideration since the early days of fracture mechanics. Here we consider a method to deal with this issue, which combines a set-valued opening-rate-dependant cohesive law, a quasi-explicit solver and the eXtended Finite Element Method of representing a crack. The approach allows a propagating crack to be mesh-independent while also being dynamically informed through a quasi-explicit solver. Several well established experiments on glass (Homolite-100) and Polymethyl methacrylate (PMMA) are successfully modelled and compared against existing analytical solutions and other approaches in 2D up until the experimentally observed branching speeds. The comparison highlights the robustness of ensuring energy is conserved globally by treating a propagating phenomenological crack-tip implicitly, while taking advantage of the computational efficiency of treating the global dynamics explicitly.

Keywords: elastodynamics; cracking; cohesive zone; XFEM; quasi-explicit scheme; velocity hardening

1. INTRODUCTION

The kinetics of crack propagation is of considerable importance in a large variety of areas from predicting crack arrest length in engineering structures, earthquakes and bone fracture, to impact fragmentation protection in spacecraft and military armour.

The majority of modelling approaches to date have assumed that the material response is independent of crack propagation [1,2,3]. This is equivalent to considering structures as time-independent continua subject to instantly applied changes in boundary conditions. In reality, materials behave differently at different length scales. This length-scale dependency ultimately leads to an element of discreetness at some material specific scale. The result is a delay in displacement propagation from application of boundary loading, to an incident point of interest, such as a crack tip. This is where the field of dynamic fracture mechanics aims to bridge the gap between material (continuum) dynamics and crack propagation (an extension of a discontinuity) by considering dynamically-loaded cracks, inertia and rate-dependent material behaviour [2].

The first analytical treatise of dynamic fracture was made by Mott, who amended the Griffith's energy balance for a central crack in an infinite plate with the kinetic energy of a fracture event. His modified expression for the strain energy release rate in an elastic continuum reads:

$$G(t) = \frac{dF}{da} - \frac{dU_E}{da} - \frac{dE_k}{da}, \tag{1}$$

where a is the crack length, F is the work done by external forces, U_E is the elastic strain energy given by:

$$U_E = U_{E_o} - \frac{\pi\sigma^2 a^2 B}{E}, \tag{2}$$

and E_K is the kinetic energy, given by:

$$E_k = \frac{1}{2}k^2\rho a^2\dot{a}^2\left(\frac{\sigma}{E}\right)^2. \tag{3}$$

In Eqns. (2) and (3), σ is the remotely applied stress normal to the crack, ρ and E are the density and Young's modulus of the material, $\dot{a}$ is the crack speed, and k is the wave constant. From Eqns. (1)-(3), Mott derived a time-dependent strain energy release rate [4]:

$$G(t) = \frac{1}{2}\frac{d}{da}\left[\frac{\pi\,\sigma^2 a}{E} - \frac{k}{2}\rho a^2 \dot{a}^2 \left(\frac{\sigma}{E}\right)\right] = 2\Gamma \tag{4}$$

where Γ is a constant specific surface fracture energy. When compared to a material parameter, i.e. critical strain energy release rate G_c, Eq. (4) provides a criterion for crack stability: for $G(t) < G_c$ the crack will remain stationary, otherwise it will extend. This can be recast into a more familiar criterion based on comparison between (time-dependent) stress intensity factor, $K_I(t)$, and plane stain fracture toughness K_{Ic}, which is related to G_c via:

$$G_c = {K_{I_c}}^2 \left(\frac{1-\nu^2}{E}\right). \tag{5}$$

Equation (4) is derived with two limiting assumptions: the crack travels at a steady-state speed; and this speed is small compared to the shear wave speed within the material. However, due to the increased kinetic energy, dynamic fracture can occur below this critical limit for non-steady state speeds. Thus, K_{Ic} can be seen as a function of the crack velocity, which may not exceed a limiting value - the Rayleigh surface wave speed c_r. Kanninen and Popelar [5] have shown that:

$$\dot{a} = c_r \left(1 - \frac{K_{Ic}}{K_I}\right) \tag{6}$$

where $\dot{a}$ is the macro-crack speed. If K_{Ic} is assumed a material constant, i.e. fracture toughness is assumed independent of strain rate, then Eq. (6) will stand up to quantitative comparison with experimental data at low propagating speeds. Through extensive experiments on Homolite-100 by Ravi-Chandar and Knauss [6], it was observed that a propagating crack does not exceed ~0.7c_r due to multiple yet not fully explained dynamic fracture features which dissipate the fracture energy beyond this limit. They also observed the crack propagation process for a fast brittle crack contained a large diffuse zone of micro-cracks ahead of the tip. This process produced an oscillating macro-crack profile, slowing down the crack, leading in some cases to macro-crack branching [6, 7].

The assumptions used by Mott for deriving Eq. (4) allow for two possible scenarios for modelling dynamic fracture:

- When a crack in a body subjected to a slowly varying load reaches a point of instability and propagates rapidly, leading to sudden unloading along a crack path. This is closer to a quasi-static situation, where the crack has a long time to dissipate energy relative to the fast propagation.

- When a body with a stationary crack is subjected to a rapidly varying load such as an impact, giving rise to high stress levels near the crack tip. This high stress level does not allow sufficient time for plastic deformations to develop before fracture, hence, energy must be dissipated by other mechanisms, e.g. micro-cracking. Therefore, energy is released within a short time frame leading to rapid crack propagation, possible sub-branching and or, macro-crack branching.

These two different scenarios have often been treated separately in fracture modelling due to the difficulty in integrating time-dependent and decaying discontinuities such as a crack in Figure 1 (a) into oscillating continuum systems under an external vibratory loading as in Figure 1(b). This is because the strain waves produced by a propagating crack are often within the same order of magnitude as the global oscillating potential, making the resolution of a propagating crack within a model numerically stiff. While the separation of these scenarios is useful for analytical treatments, in reality they maybe realised simultaneously and there is no reason to keep them separate when dynamic fracture is modelled numerically.

This paper offers a framework for numerical modelling of dynamic fracture where both scenarios are taken into account. As a first application of the framework, the dynamic crack propagation is followed up until the crack branching point, which is defined by the limit presented by Eq. (6). The post-branching behaviour is a subject of on-going work to be presented later. The developed modelling approach ensures energy conservation by allowing the energy released during crack propagation to be resolved by the global system through a quasi-explicit solver and a velocity dependent

cohesive law implemented via the eXtended Finite Element Method. The strategy is tested on two well-established experiments and discussed in relation to other available approaches to modelling dynamic fracture. The first experimental comparison allows the crack to arrest before reflected strain waves interact. The second experimental comparison includes the interaction of reflected strain waves with the propagating crack, allowing for consideration of the effects of the interacting strain waves on a propagating crack.

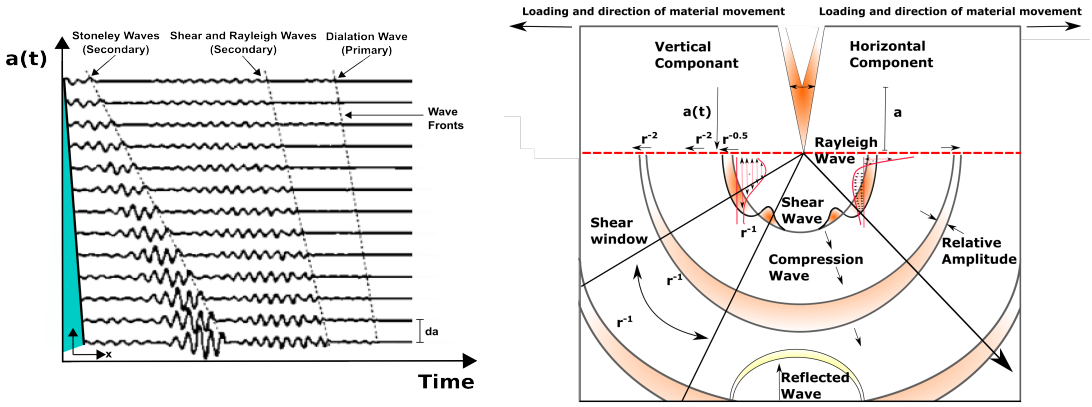

(a) **(b)**

Figure 1 – (a) Primary and secondary waves produced during dynamic propagation (locally). The Dilation waves have a higher velocity than the shear waves and Stonely waves which are caused by crack lips contacting; (b) A schematic showing the combination of shear and longitudinal waves energy dissipation within a finite geometry including the reflected waves from a previous propagation step and or external vibratory loading (globally) [1, 3].

2. MODELLING

The proposed modelling approach has three components:

1. An implicitly treated velocity dependent ‘phenomelogical’ cohesive law to represent the crack tip, implemented along the main crack path only;
2. A quasi-explicit solver to resolve the crack globally ensuring energy conservation;

3. A propagation algorithm using the eXtended Finite Element Method (XFEM) to represent the crack independent of a mesh.

The combination of these allows a propagating Fracture Process Zone (FPZ) to be integrated into a global continuum dynamic model and the energy from reflected waves to influence a propagating crack in an energetically conservative manner; effectively bypassing any numerical stiffness.

2.1 PHENOMELOGICAL RATE DEPENDENT COHESIVE ZONE

Cohesive zone models have been used in modelling dynamic fracture [8, 9, 10, 11] however, they often lead to different results, particularly when the cohesive law contains elastic branch prior to damage initiation. This is because, the initial elastic traction-separation behaviour does not allow for resolving the cohesive zone without affecting the wave speed. To overcome this, Zhou et al. [12] have suggested a more phenomenological crack-opening-rate-dependent cohesive law, which accounts for rate/velocity effects. This is introduced on the main crack path only, rather than for the micro-cracking process in the FPZ. The law has been derived from multiple experimental observations, summarised in Fig. 2. Specifically, irrespective of component geometry it has been observed that the dependence of *Gc* on the crack velocity, $\dot{a_0}$, is monotonically increasing and described with reasonable accuracy by a simple empirical expression [13]:

$$G_c(\dot{a_0}) = G_0 \, log\left(\frac{\dot{a_L}}{\dot{a_L}-\dot{a_0}}\right), \tag{7}$$

where $\dot{a}_L$ is the limiting crack velocity, and G_0 is the strain energy release rate at $\dot{a_0} = 0$. The proposed equation is clearly an approximation to the real toughness-velocity relation at the two limits: *Gc* approached zero as crack velocity $\dot{a_0}$ approaches zero (i.e. the material is very brittle compared to fast fracture); *Gc* approached infinity as crack velocity approaches the limiting value. The rapid increase of *Gc* with $\dot{a_0}$ is explained with a velocity-toughening effect of the material [14].

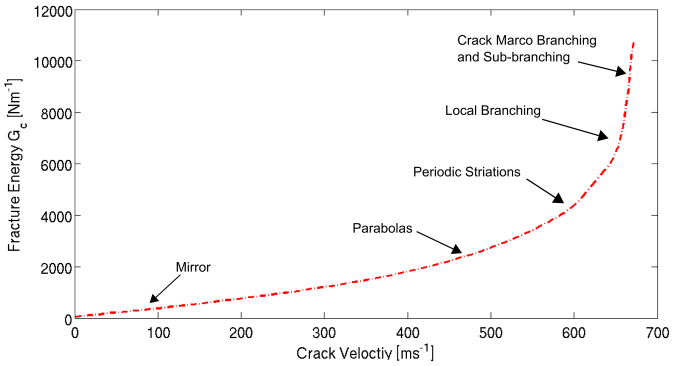

Figure 2 – Geometry independent velocity toughening curve of G_c in Equation 7 and the indicated points where dynamic fracture phenomena are observed [12].

To avoid the problem introduced by initial elastic traction-separation behaviour, we have considered a initially rigid-softening behaviour, schematically shown in Fig. 3, with toughness-velocity dependence based on Eq. (7). Since the critical stress is assumed to be independent of crack velocity, the illustrated behaviour is called opening-rate-dependent cohesive law. A fracture process zone with this law has been previously used to study crack branching [1].

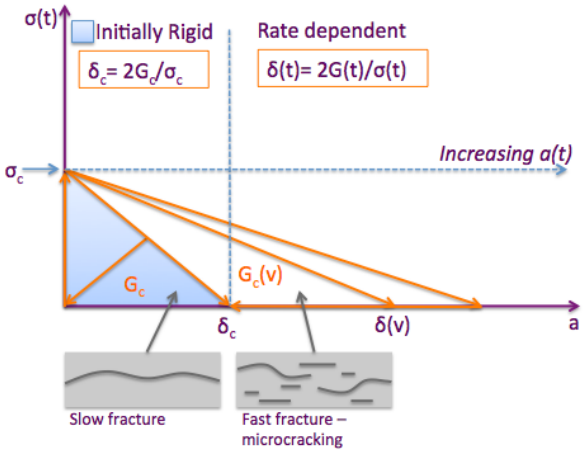

Figure 3 – An initially ridged opening-rate-dependent phenomenological cohesive law [1, 9].

Evident from the figure is that for a stationary crack (or very slow propagating crack) one needs to specify two material parameters, e.g. fracture energy and critical stress, which are related to the third, e.g. failure displacement, via

$$G_c = \frac{1}{2}\sigma_c\delta_c. \tag{8}$$

For high crack velocities, the micro-cracks developing in the fracture process zone lack time to unload each other [9]. As a result the dynamic fracture process happens in an enlarged damage zone, which dissipates more energy. With the assumption for velocity-independent critical stress, the velocity dependence of the fracture energy is equivalent to a velocity dependence of the failure displacement, given by:

$$\delta_c(\dot{a}) = \delta_0 \log\left(\frac{\dot{a}_L}{\dot{a}_L - \dot{a}_0}\right). \tag{9}$$

A cohesive zone crack representation is associated with a cohesive critical length, l_c, which is dictated by the materials elastic and failure properties; at zero velocity this is [8]:

$$l_c(v = 0) = M\left(\frac{G_c E}{\sigma_c{}^2(1-\nu^2)}\right). \tag{10}$$

Equation (10) provides an inverse measure of material's toughness: the smaller l_c, the more brittle the material and is also related to the size of a fully developed fracture process zone under a peak load at initiation, which from Rice's model has scaling factor [10, 14]:

$$M = \frac{9\pi}{32} \approx 0.88 \tag{11}$$

This limit represents the limit of the material topography resolution and therefore the limit where dynamic instability may occur. The validity of using an approach for fast fracture, where the bulk material properties accuracy breaks down at a fixed value l_c, comes from understanding of the effects of the microstructure at a lower scale on velocity hardening and crack tip momentum observed in Fig. (2). Freund suggested that the macroscopically perceived fracture energy represents the maximum rather than the average of the fine-scale resistance produced by the microstructure [2]. This is to say that if the fracture energy, Γ, in Eq. (4) has a periodic variation due to the microstructure, then the maximum variation of this governs the crack growth behaviour for speeds near $\dot{a}$=0 (initiation), but the average of the variation governs

behaviour for speeds approaching the material speed limit in Eq. (6). This suggests that for very fast cracks the microstructure significance diminishes, but becomes increasingly important as the driving force decreases. The limit l_c then allows for the G, K, COD equivalency to be satisfied through Eqns. (6) and (9), for a propagating dynamic macro-crack:

$$G_{ext} = -G_{cohesive} = \frac{1-\upsilon^2}{E}\left({K_I}^2 + {K_{II}}^2\right) + \frac{1}{2\mu}{K_{III}}^2 = \sigma_c \delta \qquad (12)$$

where G is the Linear elastic J integral [2]. The relation in Eqn. (12) allows computationally for a contour integral of G to be related to the toughness of a material through K (stress intensity factor) and then discretised through δ to integrate a discontinuity (crack) into a continuum model, using a quasi-explicit solver.

2.2 QUASI-EXPLICIT SOVLER

The difference between an implicit and an explicit time scheme comes from which part of a second-order non-linear equation, which describes a crack tips motion, is used to integrate a continuum solution. Implicit solutions are based on quantities calculated in the previous time step (backward Euler time scheme), which means even for large time steps the solution remains stable (unconditionally stable). There is a disadvantage to this however, this requires the calculation of the inverse stiffness matrix as it directly solves for the displacement vector, which is computationally intensive, especially with non-linear features present (material heterogeneity/strain waves), because the stiffness matrix itself will become a function of displacement. There is also the risk that such a highly non-linear computation may fail to converge, leading to a lack of robustness. For an explicit analysis, instead of solving for displacement, a solver resolves the solution through acceleration, bypassing the need for the stiffness matrix inversion and instead inverting the mass matrix. The mass matrix is also 'lumped' meaning the solution is easily obtained through a single step of inverting the matrix diagonals. This requires low-order elements that are preferred by explicit solvers. An explicit solver such as the Central Differences Method, illustrated by Eq. (13), is useful when resolving crack speeds from the perspective of the materials response to its propagation.

$$\dot{U}_h{}^n = \frac{U_h{}^{n+1} - U_h{}^{n-1}}{2\Delta t} \qquad \text{and} \qquad \ddot{U}_h{}^n = \frac{U_h{}^{n+1} - 2U_h{}^n + U_h{}^{n-1}}{\Delta t^2}. \tag{13}$$

This overcomes the difficulty of resolving crack velocities that may have the same order of magnitude as the waves produced in the solid, requiring a small time-step; leading to computational savings compared to resolving velocities implicitly. However, an explicit solver alone does not conserve energy and requires a forcing term, $L_h(t^n)$, from an initial implicit calculation to maintain the shifted energy polynomial [16]:

$$\varepsilon^{n+1} - \varepsilon^n = \frac{1}{2}\left(L_h(t^{n+1}) + L_h(t^n), U_h{}^{n+1} - U_h{}^n\right). \tag{14}$$

Explicit methods are also subject to a stability condition known as the Courant-Friedrichs-Lewy Condition (CFL) due to not using an Reverse Euler time scheme such that $\Delta t \leq \Delta t_c$ [18]. In comparison with implicit analyses, the number of time-steps for dynamic fracture is increased with an explicit time scheme, but the explicit inversion of the diagonal mass matrix makes the computational cost per time step much lower [16]. The critical time-step for stability should be smaller than the mesh resolution such that:

$$\Delta t_c{}^{XFEM} = \frac{\Delta t_c{}^{FEM}}{2} = \frac{h_{min}}{c_d}, \tag{15}$$

where h_{min} is the length of the smallest element length and c_d is the dilation wave speed. The time condition is half of that for a standard FEM solution to resolve the Heaviside function as XFEM crosses an element (discussed in the next section) [18]. This combination allows for a crack to be implicitly energetically stable, while an explicit solver handles the highly non-linear nature of a dynamically propagating crack in an oscillating complex geometry.

2.3 CRACK PROPAGATION ALGORITHM

The propagation algorithm, illustrated in Fig. 4(a), follows a quasi-implicit formulation of a set-valued linear-softening cohesive law introduced by Doyen et al [16] and shown in Fig. 4(b). It first computes a potential crack surface, for which it introduces a rigid cohesive zone with full adherence to avoid non-physical opening. This is then followed by the insertion of the velocity dependent cohesive law, shown in Fig. 3, to represent the velocity hardening, Eq. (7). At each time step of the calculation the interface forces are treated implicitly, particularly due to the tangential forces being discontinuous with respect to tangential opening. The tractions are then resolved explicitly by computing the intersection of the set-valued law through a Central Differences Method. This is achieved through Newton-Raphson Iterations of a Lorentz Path Following Method to resolve each intersection point of the law (Fig. 4(b)) [9]. The opening-rate-dependence of the cohesive zone model introduces a second time-scale, which is smaller than for the crack-tip speed and therefore requires smaller time steps to be resolved [1, 9].

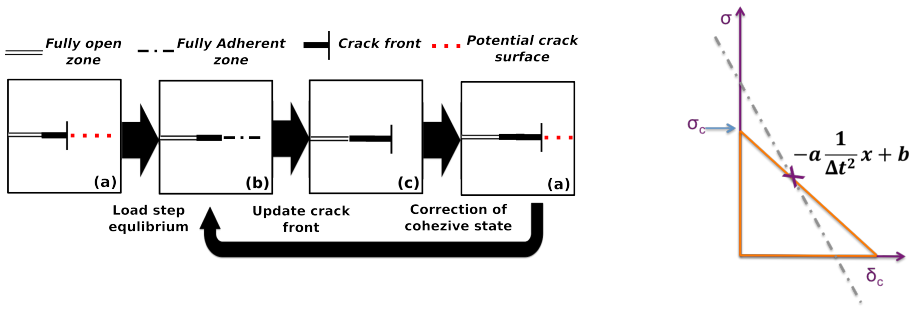

(a) **(b)**

Figure 4 – (a) Algorithm of crack propagation; (b) Analytical determination of tractions in an implicit cohesive law with an explicit time discretisation. The line crossing through the law is the intersection resolved by the Lorentz Path Following Method [9, 16].

Ferté et al [9] improved on this formulation by integrating this scheme into XFEM, enabling a dynamic crack to cross elements, effectively making the crack mesh-independent. This is to say that, if an additional length scale is provided to a model as the typical distance between two cohesive surfaces, the results become insensitive to the mesh size [8]. In essence, the macro crack is informed from the meso-scale

dynamic material effects. Hence, as long as $h_{min} < l_c$ the cohesive zone can be resolved - typically 5 or more elements in the zone. If the opening between two cohesive surfaces is such that $\delta_c >> h_{min} \leq l_c$ then the crack path can be considered independent of the mesh. It is also important to point out that the shape of the cohesive law does not significantly affect the final crack shape, meaning that the internal cohesive forces are independent of the mesh [8, 14, 15].

XFEM represents a crack through exploiting the partition of unity concept and is based on a set of nodal shape functions, whose sum is equal to one at each point in the field considered:

$$u(x) = \sum_i a_i \, N_i(x) + \sum_i b_i \, N_i(x) \, H(x) = 1 \,, \tag{16}$$

where *u(x)* is the approximated function for one element, *H(x)* is the Heaviside function (discontinuous part), $N_i(x)$ is the standard finite element function for node *i*, u_i is the unknown part of the standard finite element function, M_i is the local enrichment of node *i* and a_i is the unknown enrichment at node *i* [8]. This is where basis step functions are added to standard polynomial basis functions (enriched), at nodes that are intersected by a crack; to provide the crack opening displacement, as can be seen in Figure 5(a) [13]. The approach considered here is a quasi-explicit one, which treats a cracks FPZ as a cohesive zone implicitly, at the meso-scale, and then for the component dynamics to be resolved explicitly, at the macro-scale, through lumping the mass matrix in XFEM [9, 16]. The cohesive zone is inserted with XFEM level-sets through a smeared crack tip as in Figure 5(b). This is then used to compute the stress intensity factors and therefore the cohesive parameters through the *G*, *K*, *COD* equivalency in Equation 12.

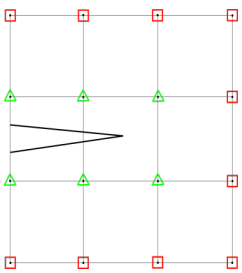

(a)

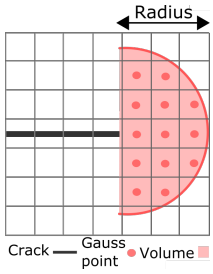

(b)

Figure 5 – (a) An XFEM representation of a crack not aligned to the mesh. The green triangle nodes are enriched with discontinuous function (Heavy-side), and red square nodes are the classical FEM part; (b) Smeared crack-tip allowing for the insertion of the cohesive zone.

2.4 ALTERNATIVE MODELLING APPROACHES

A number of different methods have been used to date to model time dependent fracture, some use discrete elements or finite volumes, but the majority use the Finite Element Methods (FEM). Classic FEM approaches such as the Nodal Release Method (NRM), Fig. 6(a), or the Element Deletion Method (EDM), Fig. 6(b), involve a significant level of mesh dependency due to the application of material degradation laws or fracture criteria, which control the process of crack initiation, propagation and/or arrest. Most modern approaches stem from either NRM or EDM and try to overcome the limitations of how closely a material's physics is represented. These approaches generally come in the form of rigid cohesive elements, Fig. 6(c), or material damage laws to represent the fracture process, and, adaptive meshing techniques such as mesh-refinement or mapping through error estimation, to overcome mesh dependency [1, 19, 20]. Cohesive elements are also limited in use by requiring predefined crack paths along element boundaries, with fixed crack opening jumps, leading to non-physical crack path representation [21].

Furthermore, time continuity is important in dynamic fracture problems, with crack advances often over large parts of a mesh, so re-meshing would need to be performed many times. Even when modelling stationary discontinuities, these methods can be quite cumbersome because construction of a mesh that adheres to the discontinuity surfaces can be difficult. Alternative approaches using discrete elements, which try and bypass this such as the Element Free Galerkin Method (EFG) or Peridynamics, Fig. 6(d), often struggle with application of boundary conditions meaning they require millions of elements to resolve discontinuities [7, 22]. This therefore makes eXtended Finite Element Method (XFEM) a more sensible choice than other approaches by bypassing the need re-mesh.

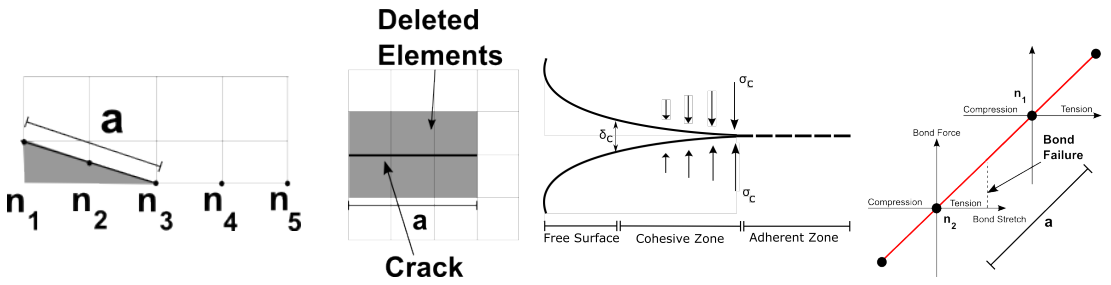

(a) **(b)** **(c)** **(d)**

Figure 6 – (a) NRM crack representation (b) EDM crack representation; (c) Cohesive zone crack representation through a cohesive law; (d) Peridynamic crack representation of a crack through an elastic bond between two discrete elements.

To examine the applicability of the quasi-explicit CZM approach proposed here for dynamic macro-crack propagation it is compared to the following previously discussed approaches [22, 23]:

1. Peridynamics (PD),
2. Dynamic Cohesive Zone Modelling (CZM),
3. Element Deletion Method (EDM),
4. eXtended Finite Element Method with a damage parameter (XFEM),
5. eXtended Finite Element Method – Cohesive Nodal Method (XFEM-CNM)

The main difference of the approach used in this work compared to previous CZM approaches is that XFEM enrichment is used to insert a crack along a pre-defined path with a phenomenological cohesive law, meaning that the crack definition is no longer purely along element boundaries. It is anticipated that the new approach will provide further insight into the nature of modelling dynamic fracture.

The examples considered in the next sections are from experiments, where the cracks were observed to follow straight paths prior to branching. Hence, in this initial application of the proposed modelling strategy, a pre-defined straight crack path is used and no external branching criterion is applied. Notably, branching criteria have been used in previous works for fine-tuning the crack profiles. In the present work

without branching criterion, the crack propagation is followed until the onset of branching/bifurcation.

4. APPLICATION 1 - PMMA

The first application investigated with quasi-explicit CZM is based on an experiment conducted by Fineberg and Sharon on a 440 by 380mm piece of Poly(methyl methacrylate) (PMMA), which is considered to have a noticeable rate-dependent fracture toughness and crack jump, Fig. 7(a) [22, 25, 26]. Furthermore, PMMA has a very high toughness, K_{Ic} or G_c, meaning that the observation of crack branching will occur at lower speeds (see Fig. 3). PMMA is also the main material used by Zhou et al [12] to produce the velocity dependent cohesive law, and ideal experiment to consider a quasi-explicit CZM crack without influence of reflected waves or external oscillatory loading.

In the experiment, an initial very small 4mm low constraint notch was introduced to the centre of one of the longer sides. The PMMA sheet was then loaded statically just below the critical limit of fracture and a sharp razor was then used to trigger propagation. The size of the geometry was considered such that the dissipated energy from the fast fracture event did not have enough time to reflect back to interact with the propagating crack before it arrested meaning the crack was purely driven by the rate-dependent fracture energy. When modelling this experiment using the quasi-explicit CZM approach, the initial material properties were chosen to be the ones used previously such that: E = 3.24 GPa, Mass Density ρ = 1190 kg/m^3, with the Rayleigh Wave speed considered to be c_r= 930 ms^{-1} [15, 23]. The initial parameters for the cohesive law were also selected to be those used previously by Song et al. and Camacho and Ortiz [10, 15, 23]: σ_c = 75MPa and $G_f = G_c$ = 500Jm^{-2}.

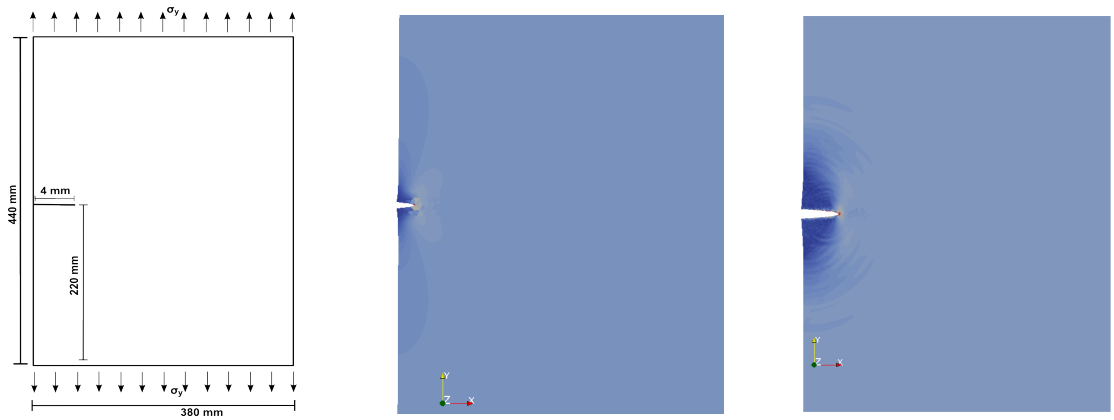

(a) (b) (c)

Figure 7 – (a) Schematic of the small blunt pre notch PMMA plate; (b) Contour stress plot of the initial small notch; (c) Contour stress plot of the finally crack.

The contor stress plots for the initial notch and final crack are shown in Fig. 7(b-c). Evidently, the waves produced by the crack do not interact with the sides of the plate and the kinetic energy is dissipated away from the propagating crack. The simulated crack velocity versus time is plotted in Fig. 8, together with the experimental results and simulations with other modelling approaches, including: XFEM, Peridynamics and fixed jump CZM.

It can be seen in Fig. 8 that using quasi-explicit CZM approach, with G_c= 500 Jm^{-2}, agrees very well with the experimental crack velocity, particularly at later stages where the crack-tip acceleration is low just before macro-crack branching which was observed in the experiment at around 80μs. This good correlation is obtained despite following an assumed straight crack path. The closest of the previous methods is XFEM with an external damage parameter, but the proposed quasi-explicit CZM approach is seen to perform better, because by being dynamically informed the crack velocities are more realistic and mesh independent. The oscillations in the experimental crack speed are due to the large strain rate crack jumps which tapper out at lower gradients as observed by Song et al [23].

The key difference between the quasi-explicit CZM approach and the standard CZM is that the former uses rigid-softening cohesive law, while the latter uses elastic-softening law. Song et al [23] argued that the pre-damage elastic branch was appropriate to introduce some hardening that accounts for initial plasticity due to crack initiation. However, in a propagating dynamic crack there is little time for the

material to respond plastically before the next fracture event. Hence, the initial elastic branch appears to be less realistic at higher fracture speeds seen just after initiation, and this is illustrated by the good correlation between experiment and simulations with rigid-softening cohesive law (quasi-explicit CZM).

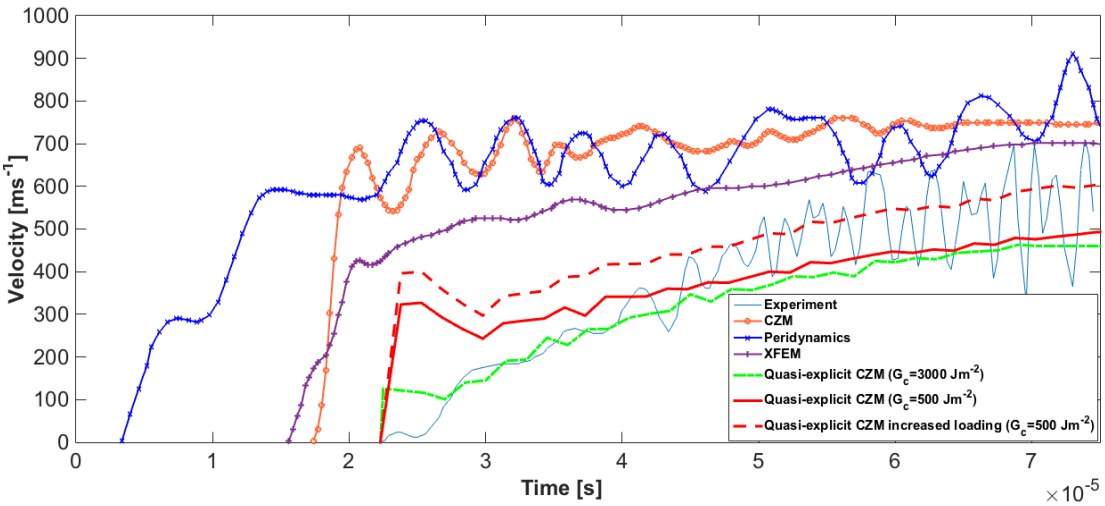

Figure 8 – Comparison graph of crack displacement-time profiles including: experimental data, XFEM, fixed jump CZM, Peridynamics and quasi-explicit CZM for G_c= 500 Jm^{-2} and G_c = 3000 Jm^{-2}.

The other modelling approaches can be seen to clearly over-estimate the crack velocity early on in the crack onset while trying to capture the micro-cracking profile, which is almost straight throughout the propagation. Also, just after the crack initiation is where the strain-rate-dependency of the fracture toughness of PMMA will be significant due to it being a polymer. Previously, Song et al suggested that PMMA's experimentally measured fracture toughness maybe six times larger, i.e. at G_c= 3000 Jm^{-2}, after fitting the model to the experimental results [23]. The quasi-explicit CZM result with this fracture energy is also shown in Fig. 8 and fits better at the onset of the crack where there is greater energy dissipation and therefore a more rate-dependent crack jump. The profile then converges with the previous experimentally observed critical fracture toughness of G_c= 500 Jm^{-2}. This demonstrates that PMMA's fracture may have some strain rate dependency, which cannot be accounted for by an increased static loading when using G_c= 500 Jm^{-2}. As demonstrated by Fig. 8, the other approaches are not able to capture this behaviour.

4. APPLICATION 2 - PRE-NOTCHED GLASS

The second application considered by this quasi-explicit CZM approach, is based on an experiment by Ramul and Kobayashi and has been used for many model comparisons previously, Fig. 9(a) [9, 23, 27]. In the experiment, a piece of Homolite-100 in a Double Cantilever Beam (DCB) configuration, Fig. 9(b), with an initial high constraint blunt notch, was exposed to a loading and the subsequent fracture patterns observed. Homolite-100 has a low fracture toughness KI_c/G_c meaning that crack branching will be observed at much higher speeds (see Figure 3), closer to its c_r than PMMA as the crack-tip has less momentum. This application allows for strain waves to interact with the propagating crack to observe further the rate-dependent effects of interacting strain waves.

The initial material properties for this were known to be: a Young's modulus of E=32GPa, a Poisson's ratio υ = 0.2, a mass density of ρ = 2450 kg/m^3 and also an applied loading in the materials y-axis direction of σ_y = 1 MPa.

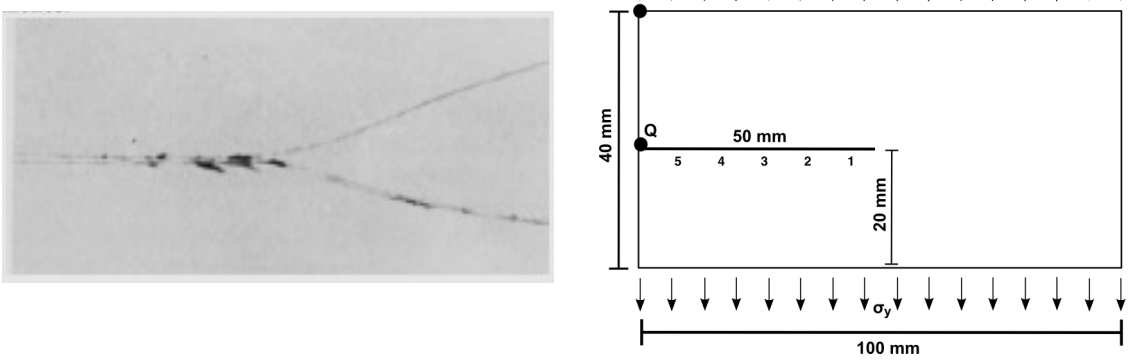

(a) **(b)**

Figure 9 - (a) Experimental image from Ramul and Kobayashi [26]; (b) DCB schematic showing the initial blunt notch.

After a period of self-similar crack growth it was observed in the experiment that the crack branched (t_b~39μs). This has been believed to be due to the crack reaching a speed of approximately 0.72C_r such that the excess energy dissipates through a secondary crack. In modelling terms, this point represents the limit between internal energy driven fracture and the fast transient simulations above this limit where excess external energy exists in the system. The aim of this second problem is to probe this

experiment using the method described previously to consider the effect of rate dependent loading on the prediction of the crack branching time. To do this, three model arrangements are considered: firstly a model under static loading which has an analytical solution to accompany it, secondly a double crack configuration to observe the effects of crack arrest due to the presence of a second dynamic crack or reflected waves and finally, under a step-loading similar to that used by Song et el for a non-opening-rate-dependent (standard) CZM previously [23, 28].

4.1 STEADY-STATE DCB ANALYTICAL SOLUTION

The first loading regime used a static load of 1 MPa in the y-axis direction of the DCB in Fig. 9(b). This regime is known to produce a steady-state dynamically propagating straight crack (after an initial acceleration) and was considered analytically by Freund [28] who provided one of the first full analytical solutions to dynamic crack propagation. It is based on taking invariant contour integrals of a cohesive zone model of a known geometry, which allows for the calculation of the global energy state. The solution is based on a low constraint sharp crack under linear elastic fracture assumptions and considers the crack to be a point particle traveling through the materials phase-space which interacts with reflected waves. The solution follows the 1D string problem while considering the crack-tip to be a collection of excitations, which decays in the materials phase space, i.e. a quasi-particle.

The propagation of a sharp crack in a DCB is described by a second order differential equation:

$$\ddot{a} = \frac{1}{2}\frac{\dot{a}^2}{a} + \frac{105}{4}\frac{EI}{\rho A}\frac{1}{a^3} - \frac{35}{12}\frac{\Gamma a}{\varpi_0{}^2 \rho A}, \tag{17}$$

where $G = \Gamma$ is the assumed crack growth criterion, A is the DCB area, and I is the DCB's Moment of Inertia ($I = \frac{bh^3}{12}$) and Γ_o being the strain stored per unit length given by [10]:

$$\Gamma_0 = \frac{(1-v^2)\sigma^2 h}{2E} = \frac{(1-v^2)P^2 h}{2EL^2D^2}, \tag{18}$$

where D is the plates thickness. When considering the strain energy release rate to be:

$$G = \frac{9\Gamma_0{}^2 EI}{a_0{}^4}, \tag{19}$$

and that this is equal to $n\Gamma$, n being a dimensionless coefficient accounting for some initial bluntness of the crack tip then, Equation (17) can be reduced to find the equilibrium point of crack arrest length at $\ddot{a} = \dot{a} = 0$ to approximately be [28, 29]:

$$a = a_0 n^{\frac{1}{4}}, \tag{20}$$

where a_0 is the initial notch length. The initial blunting parameter, n, in this case is a measure of the actual pre-propagation energy in excess of the minimum pre-propagation energy for a sharp crack [30].

3.2 STATIC QUASI-EXPLICIT CZM RESULTS

The material properties used for the model are σ_c = 28MPa and G_c= 3Jm^{-2} which is equivalent to Song et al; δ_c being determined by the initially fully adherent part of the velocity dependent cohesive law, Eq. (8) [15, 25]. Figure 10 shows the stress plots for a DCB under static loading ($\sigma_{max} = \sigma_c$) for Homolite-100, where Fig. 10(a) is the initial state of the notch just prior to propagation and Fig. 10(b) is just before the first reflective wave off the top and bottom loading edges of the DCB interact with the propagating crack tip, showing the initial rapid crack growth.

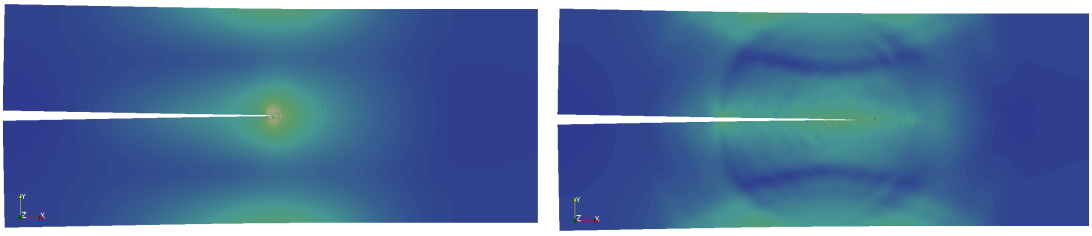

(a) **(b)**

Figure 10 - (a) A contour stress plot of the DCB initially; (b) and of crack just before the first reflected wave interacts with the propagating crack.

If the propagating crack is considered without the additional energy from the interacting strain waves then after a period of rapid growth the crack will eventually decay until rest. This can be seen as the 'analytical solution' in Fig. 11(a) [23]. However, when correcting the analytical velocity to include the strain wave increase of G and therefore crack velocity the profile reaches the experimentally observed steady-state crack velocity. This can be seen as the 'analytical solution - corrected' in Fig. 11(a) [23].

Within Fig. 11(a) the dot-dash line is where the maximum crack velocity is assumed at $0.72c_r$ where c_r is the materials Rayleigh Wave speed ~2121 ms^{-1}. It is evident that the quasi-explicit CZM crack velocity does not reach the branching point under a static loading. This point is depicted by the intersection between the maximum crack velocity and the vertical solid black line, which is the time when macro branching is observed. The quasi-explicit CZM results are also plotted against a conventional CZM model undertaken by Song et al which used a fixed δ_c and is known to agree with the corrected analytical solution and experimentally observed steady state crack speed of $0.32c_r$ [27, 28].

Under a static loading, the deflection of the upper arm of the DCB can be plotted in time as shown in Fig. 11(b). It can be seen that the opening-rate-dependence even under the static loading regime produces a significantly longer crack than the quasi-static solution, which can be calculated from the static DCB deflection relationship [31]:

$$\frac{\delta}{P} = \frac{4a^3}{Ebh^3}\left\{1 + \frac{3\sqrt{5}}{4}\left(\frac{h}{a}\right) + \frac{2}{3}\left(\frac{h}{a}\right)^2 + \frac{3\sqrt{5}}{16}\left(\frac{h}{a}\right)^3\right\}. \quad (21)$$

This also suggests that the maximum deflection of the arm is at least 2.5 times larger than if the DCB is considered under a quasi-static regime.

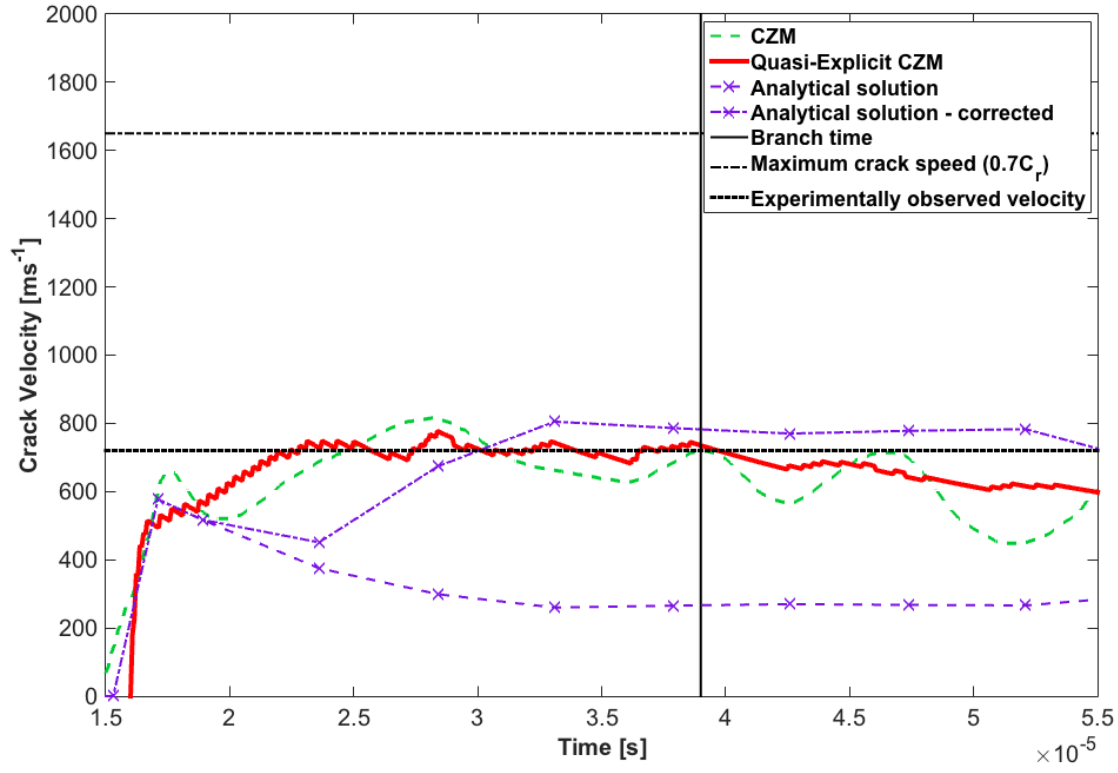

(a)

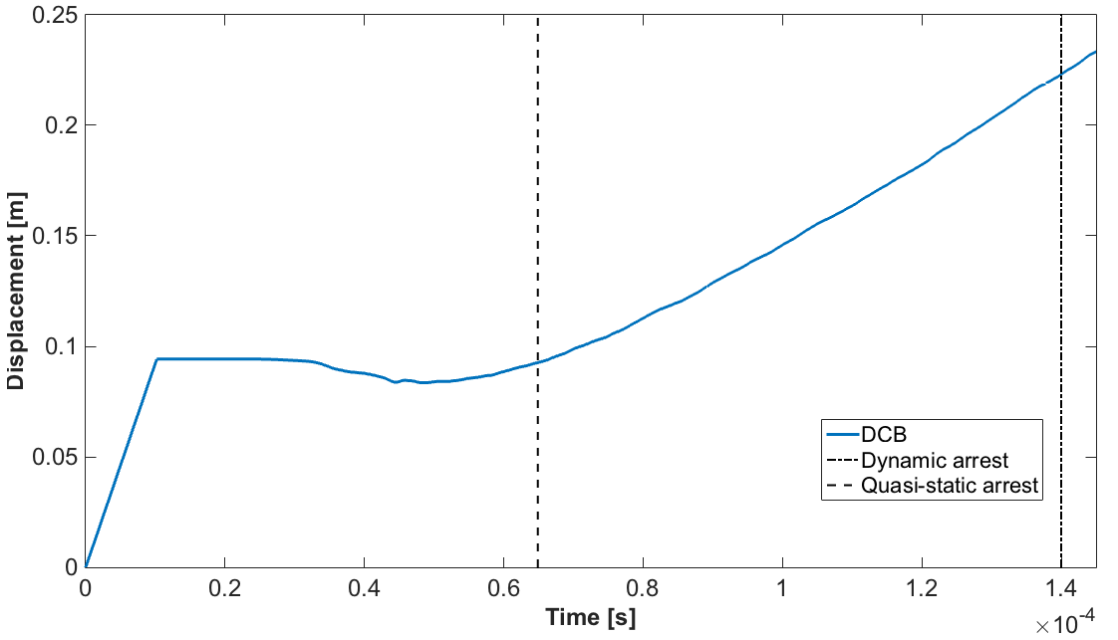

(b)

Figure 11 - (a) A comparative graph of the DCB under static loading, including CZM by Song et al and the analytical solution by Freud [23, 28]; (b) The time displacement of P in the DY direction with the quasi static and dynamic points of arrest.

The global behaviour of the DCB is illustrated in Fig. 12 using the time evolution of select displacements. Firstly, Fig. 12(a) shows the opening displacements of several equidistant points along the initial notch's arm. The results show distinctly the energy dissipation features of a component under non-linear dynamic loading from a propagating crack (compare to Fig. 1). The sharp peak is the Rayleigh surface wave, which is immediately followed by the shear bulk wave (secondary waves) and preceded by the dilation wave (primary waves). This is further demonstrated in Fig.12(b), where the displacements of the furthest point away from the notch, point Q in Fig. 8(b) are plotted. The pressure wave in the x-axis direction is ahead of the Rayleigh wave peak, which occurs when there is a perturbation in the y-axis. These waves are also followed by Stonely waves due to the crack surfaces contacting each other.

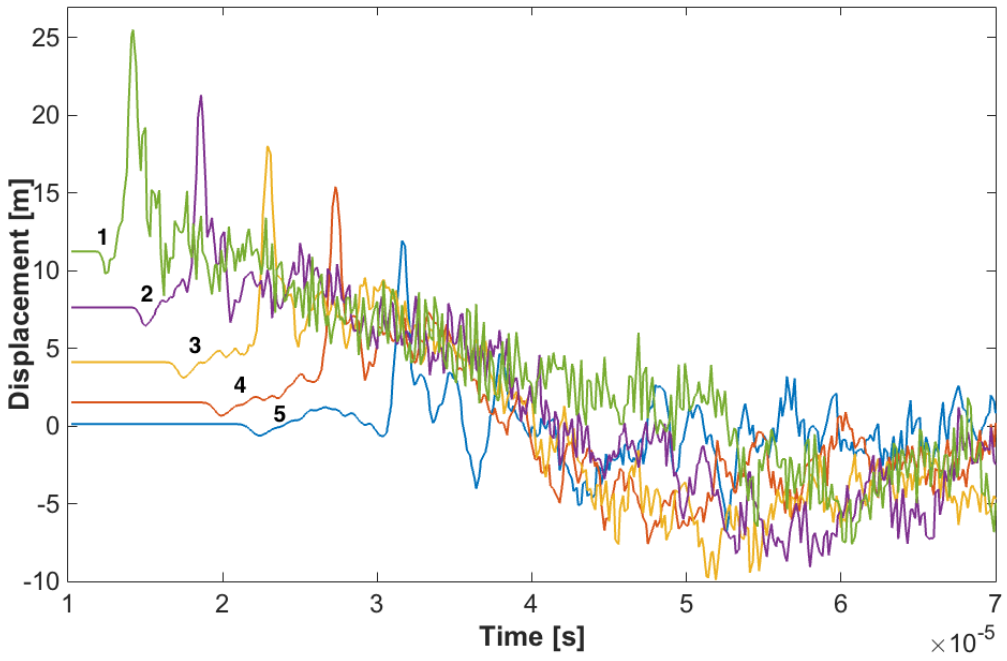

(a)

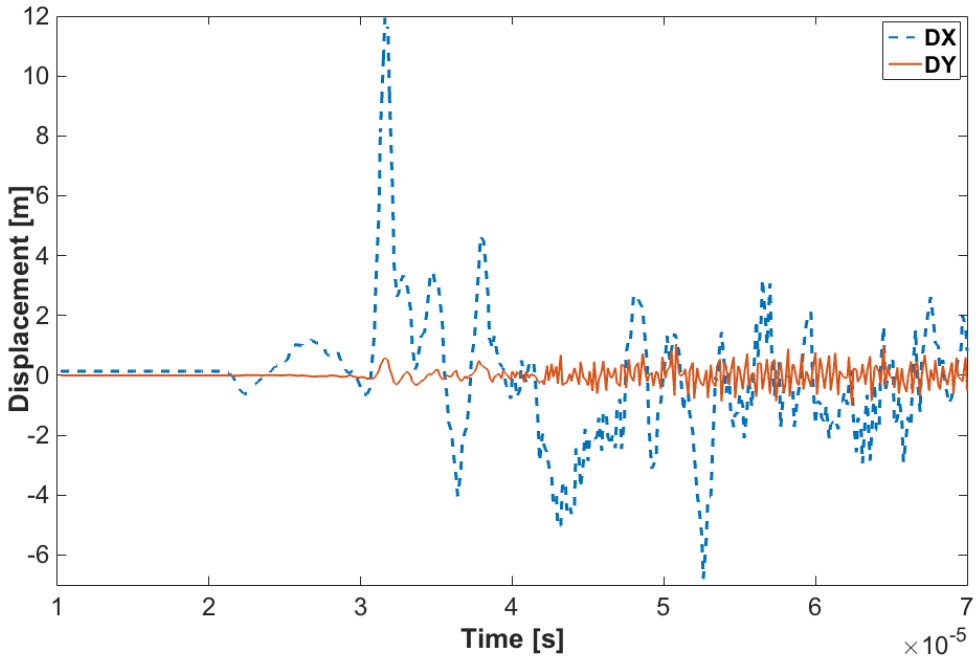

(b)

Figure 12 - (a) Time plots of Y displacement at equidistant points along the upper edge of the initial DCB notch as highlighted in Figure 9(b); (b) The x and y components of the displacement plots for point Q in Figure 2(b).

The global dynamic features from the dynamic loading of a propagating crack are evident in Fig. 12. This suggests that the cohesive crack is integrated well into a macro/component model, including correct energy conservation between solid dynamics and a propagating crack.

3.3 Straight Axial Mirrored Double Crack

It has been previously noted by Freund [28] that after crack arrest predicted by Eq. (20) and Fig. 11(b) highlighted by the dot-dash line – the displacement still increases due to the time delay in displacement/reaction, the crack may still propagate due to the DCB now being in an oscillatory state from the rate-dependent crack growth impulse (without viscous damping). This will produce a period of 'stop-start' crack propagation where the crack may close and then propagate further. This is especially so when considering an un-damped system because the component is still in an oscillating state after initial crack arrest, as seen previously in Figure 12.

For analysis of such an oscillatory propagation, a second geometry is considered in Fig. 13. This is a mirror reflection of the DCB, where the system has geometric and loading symmetry but with two dynamically propagating cracks. The setup produces double the E_k for each instance of crack increment. Each crack after a period of time (incubation time), is propagating through an undulating periodic potential due to pressure and shear waves from the other crack rather than the lower amplitude waves that reflect off the end of the DCB from a single crack.

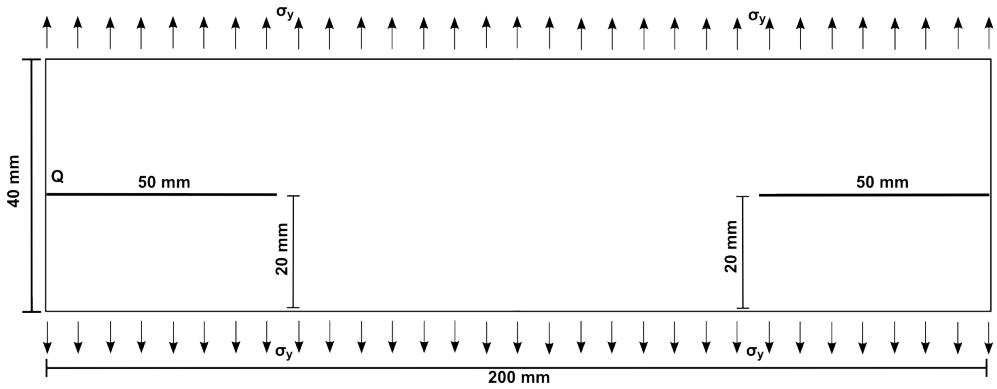

Figure 13 – A schematic of the mirrored double crack using the same parameters as in the previous DCB.

Figure 14 shows the crack tip profiles along the axis for the double crack, single crack cantilever beam and the analytical solution for the single DCB. Under quasi-static analyses, the overall component stress state is instantly changed so that each crack affects the other instantaneously. However, in a dynamical system there is a time delay, so that the two cracks do not interact until the first wave reflection. This moment is shown by the dotted line in Fig. 14, where the analytical crack speed increases. After this point the crack tip in the single DCB breaks through the end of the beam and relaxes back to the equilibrium crack arrest position. The break-through should be accepted as complete rupture of the specimen, while the relaxation is reclosing the crack and producing Stonely Waves from the interacting crack surfaces (known as 'chattering'), seen in Fig. 12(a). The region where the crack settles is bounded by arrest positions for sharp crack and fully blunt notch, which are depicted in the figure. Comparing this to the double crack system where the cracks do not significantly interact until they get close to each other (around 20 mm between them), it can be seen that the double crack does not break through completely before coming

to rest at the equilibrium arrest point. The arrest region is equivalent for both models due to the symmetry. However, the delay in energy propagation in the case of double crack makes the difference in the predictions: the component fully disintegrates by a single crack and remains intact by two cracks. This is because the energy produced by the dilatation waves reflecting of the DCB end for the single crack does not significantly alter the crack tip energy state, whereas the shear waves in the double crack system carrying the majority of the energy are enough to arrest the crack. Specifically, in the double crack system there is no free surface for the energy to dissipate over, whereas the single cracks shear wave energy is carried away by the Rayleigh wave at the surface.

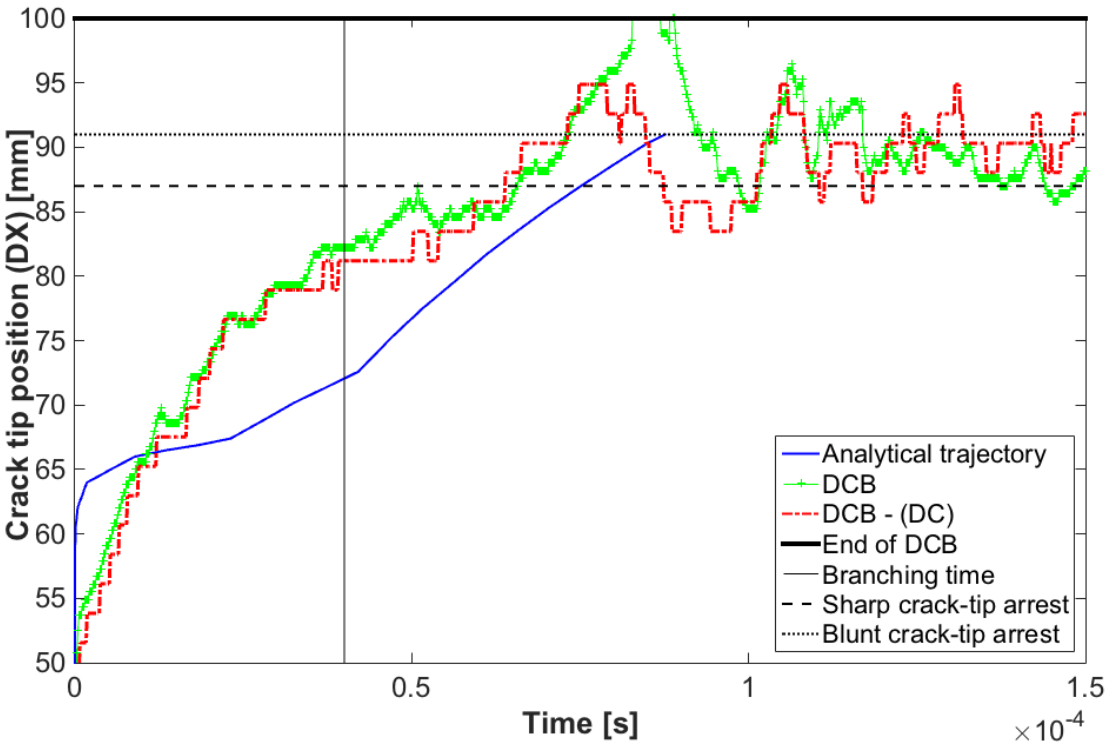

Figure 14 – Crack tip trajectories along the x-axis for the analytical solution (first wave reflection corrected), double crack and single DCB crack, highlighting the region where crack arrest is expected analytically.

The physical realism of the results, with the discussion above, demonstrates that the quasi-explicit solver corrects the energy state between the local crack tip and global system. In particular, the model captures the difference between single and double crack DCB, reflecting the specifics in their boundary configurations.

3.4 Step loading

After demonstrating that rate-independent loading produces experimentally verified and physically realistic crack speed and profile, the DCB has been subjected to a small step loading. This is from just below the σ_c to just above, similarly to the XFEM-CNM model and previous CZM model. The result for crack speed evolution up until the crack branching point is shown in Fig. 15, together with several previously published results [15, 23]. The crack branching time is depicted by the vertical dashed line and understood as the time when the first reflected strain wave interacts with the crack tip, causing an unstable decay of the crack energy state by splitting into two or more cracks.

The quasi-explicit CZM approach predicts the crack branching point exactly as experimentally measured. The fixed-step CZM and Peridynamics models predictions are ~39μs, which is where the crack tip reaches the critical branching speed of $0.72c_r$. The small oscillations in quasi-explicit CZM are in line with Zhou et al [14] initial study on opening-rate-dependent cohesive zone models. These are more significant during the onset of the crack due to the crack jumps being quite large but decay as the crack starts to decelerate. The quasi-explicit CZM profile can be seen to follow the XFEM profile but predicts the branching time more accurately. This improvement is due to the crack being fully dynamically informed as it propagates leading to a branching time predication in line with the fully discrete particle Peridynamic model. It also improves on the XFEM-CNM model by overcoming some of the mesh dependency alluded to by Agwai [15] because this approach cannot cross elements. The XFEM-CNM model also does not include the rate-dependence of the crack opening within its cohesive law meaning that it does not quite reach the critical speed, as with the Peridynamic model. Another improvement of the proposed approach, compared to the XFEM-CNM, is that extra nodes along element edges are not needed; their introduction may cause errors in the evaluated stress state. The 'bond-based' Peridynamics model has problems with the direct application of the initial static loading conditions and with resolving compressive stresses accurately [22].

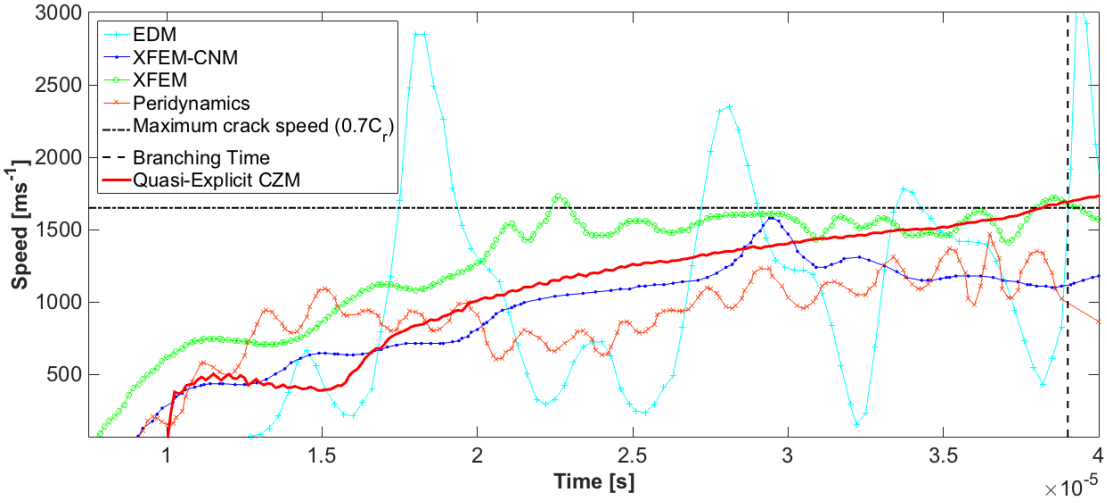

Figure 15 - Comparative graph of EDM, XFEM-CNM, Peridynamics against quasi-explicit CZM [24, 32]

5. DISCUSSION

In the applications presented above the crack paths were assumed straight for both experiments modelled. This was done because the cracks were observed to remain straight in the experiments before sub-branching and macro-crack branching was observed.

In the application to PMMA, the bulk material properties were assumed constant, while the cohesive law used a velocity-independent critical stress, σ_c, and velocity-dependent fracture energy, G_c, translating into velocity-dependent failure separation, δ_c. From another side, the material properties of PMMA are known to be strain-rate dependent. This has been shown to cause the onset of Mode-II induced sub-branching at some critical speed (around $0.4c_r$ in PMMA) [26, 33, 34]. The quasi-explicit CZM approach only considered the first ~80μs up until the sub-branching point. Within its assumptions, it predicted the speed and time expected for sub-branching to occur. While highlighting where the strain-dependent properties may change the crack velocity evolution, it appeared that the constant bulk properties were sufficient to capture this evolution accurately. Furthermore, the possible 10-15% strength increase observed in ceramics by Zhou et al [35] when increasing the strain-loading rate by three orders of magnitude is minor compared to the fracture energy released by a propagating crack. This means that the overall macro crack momentum maintains a

straight crack path through this microstructural dominant process until interaction from reflecting strain waves globally.

The application to Homolite-100, DCB subjected to step loading, allowed for the observation of the point at with macro-cracking may occur at the predicted crack speed and experimentally observed time. Also in the static double crack configuration, the observation of interacting strain waves arresting the crack demonstrated that the quasi-explicit set-valued cohesive law approach allows kinetic energy to be transferred between the crack-tip locally and oscillating system globally, while reducing the mesh dependency of the result using XFEM crack representation.

The positions for which branching is predicted in each application can be seen as the point in time where the macro-crack reaches terminal velocity. This is also where the reaction of the material ahead of the crack to the impact of released strain energy is slower or equal to the macro-crack speed. Therefore this is the point where kinetic energy becomes more important than the observed texture from the undulating potential from the microstructure. From this, there are 5 distinct phases of dynamic macro-crack propagation including those discussed by Rabczuk et al [36]:

- **Phase 1 – Initiation (Local) –** Microstructural texture is significantly noticed by a propagating crack at low kinetic energy in the system ($a << a_c$). This is seen as the linear part in Fig. 3.

- **Phase 2 – Acceleration (Transition) –** A period where the kinetic energy increases causing microstructural instability and sub-branching at a critical speed ($a \approx a_c$). This is seen as the onset of the non-linear part of Fig. 3.

- **Phase 3 – Terminal Velocity (Global)** – A period of steady state crack growth where the crack is at approximately at its terminal velocity. When strain waves interact with the propagating crack, the strain-rate energy (G) available to the crack tip is increased and the crack velocity is pushed above the critical branching speed and macro-branching is observed. This excess energy can come from either reflected strain waves from the propagating crack

or due to a rate dependant loading of the system. This can be seen as the cracks G being temporarily increased and pushing it into the branching region of Fig.3 ($a \geq a_c$).

- **Phase 4 - Deceleration (Transition) –** the crack looses momentum due to the interaction with strain waves de-constructively interacting more intensely due to the presence of a boundary, material defects or lower loading ($a < a_c$).

- **Phase 5 - Arrest (Local) –** As the crack slows the microstructural texture becomes more significantly noticed by the propagating crack, meaning a reduction in kinetic energy or the crack breaks through the boundary of the structure ($a \approx 0$).

5. CONCLUSIONS

An approach to modelling phenomenologically accurate dynamic fracture up until the crack branching speed was presented. This used an initially rigid and fully adherent implicit opening-rate-dependent cohesive law, within an explicit time stepping scheme (quasi-explicit). The approach allowed for the law to be introduced into a global model through XFEM, minimising the mesh dependency often seen with standard CZM approaches. To demonstrate how the approach builds on previous work, two well-established applications in 2D were considered from experiments and compared to previous modelling approaches and available analytical solutions.

The results from the two applications demonstrated that the quasi-explicit CZM, which represents the local micro-cracking process effects on the macro-crack, enables a more stable and energetically realistic crack velocity evolution to be followed up until the crack macro branching point. This could be the moment of sub-branching observed in PMMA (locally) or macro-branching due to strain waves in Homolite-100 (globally). The method thus allowed the global system to be loaded in a more realistic manner and to observe the effects of primary and secondary waves. This is important for computationally efficient analysis of: dynamic fracture effects on a whole component scale; stress amplification remotely from an initial crack, which may

cause subsequent crack initiations; and propagating crack under external oscillating loading.

The proposed approach brings meso-scale material phenomena into a global dynamic model enabling the analysis of fast fracture on stress amplification within structures. Further, work will look to extend this to consider flexural effects and dynamic effects on the macro crack shape in 3D and to consider the introduction of bifurcation and branching criteria due to micro-structural instability.

ACKNOWLEDGMENTS

Crump would like to thank the on-going support of EPSRC through the Engineering Doctorate Training Centre, Grant EP/G037426/1, the Dalton Nuclear Institute, and the insight given by his previous and current supervisors at the University of Manchester in producing this work. This work was also done as part of an Innovate UK collaborative project between EDF Energy R&D UK Centre, EDF Energy Generation, EDF R&D in France and the University of Manchester. The authors gratefully acknowledge EDF Energy Generation for their valuable input data and support. The views expressed in this paper are those of the authors, and not necessarily those of EDF Energy Generation. Technical support for this work from EDF R&D is highly appreciated.

REFERENCES

[1] Crump T, Ferté G, Mummery P, Jivkov A, Martinuzzi P. Dynamic fracture effects on remote stress, SMiRT-23, 2015.

[2] Freund L. B, Hutchinson J. W. Dynamic Fracture Mechanics. Journal of Applied Mechanics. 1992. p. 245.

[3] Meyers MA. Dynamic Behavior of Materials. Hoboken, NJ, USA: John Wiley & Sons, Inc.; 1994.

[4] Mott NF. Fracture of Metals: Theoretical Considerations. Engineering. 1948;165:16–8.

[5] Kanninen. M.F. and C.L. Popelar. Advanced fracture mechanics. *Oxford*

University Press; 1985.

[6] Ravi-Chandar K, Knauss WG. An experimental investigation into dynamic fracture: II. Microstructural aspects. Int J Fract. Kluwer Academic Publishers; 1984 Sep;26(1):65–80.

[7] Agwai A, Guven I, Madenci E. Predicting crack propagation with peridynamics: a comparative study. Int J Fract. 2011 Sep 4;171(1):65–78.

[8] Falk ML, Needleman A, Rice JR. A critical evaluation of cohesive zone models of dynamic fracture. Le J Phys IV. 2001 Sep;11(PR5):Pr5–43 – Pr5–50.

[9] G. Ferté, "Numerical simulation of cracks and interfaces with cohesive zone models in the extended finite element model, with EDF R&D software", PhD thesis, University of Nantes, 2014.

[10] Camacho GT, Ortiz M. Computational modelling of impact damage in brittle materials. Int J Solids Struct. 1996 Aug;33(20-22):2899–938.

[11] Xu X-P, Needleman A. Numerical simulations of fast crack growth in brittle solids. J Mech Phys Solids. 1994 Sep;42(9):1397–434.

[12] Zhou F, Molinari J-F, Shioya T. A rate-dependent cohesive model for simulating dynamic crack propagation in brittle materials. Eng Fract Mech. 2005 Jun;72(9):1383–410.

[13] Areias PMA, Belytschko T. Analysis of three-dimensional crack initiation and propagation using the extended finite element method. Int J Numer Methods Eng. 2005 Jun 7;63(5):760–88.

[14] Tvergaard V, Hutchinson JW. Effect of strain-dependent cohesive zone model on predictions of crack growth resistance. Int J Solids Struct. 1996 Aug;33(20-22):3297–308.

[15] Elices M, Guinea GV, Gómez J, Planas J. The cohesive zone model: advantages, limitations and challenges. Eng Fract Mech . 2002 Jan ;69(2):137–63.

[16] Doyen D, Ern a., Piperno S. Quasi-explicit time-integration schemes for dynamic fracture with set-valued cohesive zone models. Comput Mech. 2013;52(2):401–16.

[17] Courant R, Friedrichs K, Lewy H. On the Partial Difference Equations of Mathematical Physics. IBM J Res Dev. 1967 Mar;11(2):215–34.

[18] Menouillard T, Réthoré J, Moës N, Combescure A, Bung H. Mass lumping strategies for X-FEM explicit dynamics: Application to crack propagation. Int J Numer Methods Eng. 2008 Apr 16;74(3):447–74.

[19] Swenson D V, Ingraffea AR. Modeling mixed-mode dynamic crack propagation Using finite elements: Theory and applications. Comput Mech. 1988;3(6):381–97.

[20] Martha LF, Wawrzynek PA, Ingraffea AR. Arbitrary crack representation using solid modeling. Eng Comput. 1993;9(2):63–82.

[21] Williams C, Love. B. Dynamic failure of materials: A review. Army Research Laboratory, 2010.

[22] Madenci E, Oterkus E. Peridynamic Theory and Its Applications. New York, NY: Springer New York; 2014. 289 p.

[23] Song JH, Wang H, Belytschko T. A comparative study on finite element methods for dynamic fracture. Comput Mech Springer-Verlag. 2008;42(2):239–50.

[24] Agwai A, Guven I, Madenci E. Predicting crack initiation and propagation using XFEM, CZM and peridynamics: A comparative study. Electronic Components and Technology Conference (ECTC), 2010 Proceedings 60th.2010.p.1178–85.

[25] Mulliken AD, Boyce MC. Mechanics of the rate-dependent elastic–plastic deformation of glassy polymers from low to high strain rates. Int J Solids Struct. 2006;43(5):1331–56.

[26] Fineberg J, Sharon E. Confrming the continuum theory of dynamic brittle fracture for fast cracks. Nature. 1999 Jan 28;397(6717):333–5.

[27] Ramulu M, Kobayashi a. S. Mechanics of crack curving and branching - a dynamic fracture analysis. Int J Fract. 1985;27(3-4):187–201.

[28] Freund LB. A simple model of the double cantilever beam crack propagation specimen. J Mech Phys Solids. 1977 Feb; 25(1):69–79.

[29] Kalthoff JF, Winkler S, Beinert J. Dynamic stress intensity factors for arresting cracks in DCB specimens. Int J Fract. 1976;12(2):317–9.

[30] Lee SS, Williams JH, Kousiounelos PN. Double cantilever shear beam model of dynamic fracture in unidirectional fibre composites. Fibre Sci Technol. 1982 Sep;17(2):99–122.

[31] Kanninen MF. A dynamic analysis of unstable crack propagation and arrest in the DCB test specimen. Int J Fract. 1974 Sep;10(3):415–30.

[32] Moës N, Dolbow J, Belytschko T. A finite element method for crack growth without remeshing. Int J Numer Methods Eng. John Wiley & Sons, Ltd.; 1999 Sep 10;46(1):131–50.

[33] Zhou F, Molinari J-F. Stochastic fracture of ceramics under dynamic tensile loading. Int J Solids Struct. 2004;41(22):6573–96.

[34] Ravi-Chandar K, Knauss WG. An experimental investigation into dynamic fracture: III. On steady-state crack propagation and crack branching. Int J Fract. Martinus Nijhoff, The Hague/Kluwer Academic Publishers; 1984;26(2):141–54.

[36] Rabczuk T, Song J-H, Belytschko T. Simulations of instability in dynamic fracture by the cracking particles method. Eng Fract Mech. Elsevier Ltd; 2009 Apr;76(6):730–41.